

Dynamic Spectrum Mixer for Visual Recognition

Zhiqiang Hu
Tao Yu

ZHIQIANGHU2021@GMAIL.COM
YUTAO@MOBILE.EE.TITECH.AC.JP

Abstract

Recently, MLP-based vision backbones have achieved promising performance in several visual recognition tasks. However, the existing MLP-based methods directly aggregate tokens with static weights, leaving the adaptability to different images untouched. Moreover, Recent research demonstrates that MLP-Transformer is great at creating long-range dependencies but ineffective at catching high frequencies that primarily transmit local information, which prevents it from applying to the downstream dense prediction tasks, such as semantic segmentation. To address these challenges, we propose a content-adaptive yet computationally efficient structure, dubbed Dynamic Spectrum Mixer (DSM). The DSM represents token interactions in the frequency domain by employing the Discrete Cosine Transform, which can learn long-term spatial dependencies with log-linear complexity. Furthermore, A dynamic spectrum weight generation layer is proposed as the spectrum bands selector, which could emphasize the informative frequency bands while diminishing others. To this end, the technique can efficiently learn detailed features from visual input that contains both high- and low-frequency information. Extensive experiments show that DSM is a powerful and adaptable backbone for a range of visual recognition tasks. Particularly, DSM outperforms previous transformer-based and MLP-based models, on image classification, object detection, and semantic segmentation tasks, such as 83.8 % top-1 accuracy on ImageNet, and 49.9 % mIoU on ADE20K.

1. Introduction

Convolutional Neural Networks (CNNs) based backbones [He et al. \(2016\)](#) have dominated computer vision over the last decade. Recently, inspired by Transformer [Vaswani et al. \(2017\)](#), which achieves superior performance in natural language processing, many researchers propose to transfer the transformers into visual recognition tasks e.g., ViT [Dosovitskiy et al. \(2020\)](#), DeiT [Touvron et al. \(2021\)](#), and also attained state-of-the-art performance.

More recently, to involve less inductive bias, the MLP-based token Mixer [Tolstikhin et al. \(2021\)](#); [Touvron et al. \(2022\)](#), has taken a step forward to entirely abandoning the self-attention layer from the transformer, only employ the channel projections and spatial projections with static parameterization to mix the tokens. Despite the MLP-mixer has achieved promising results in several vision tasks [Chen et al. \(2021\)](#); [Hou et al. \(2022\)](#); [Tolstikhin et al. \(2021\)](#); [Yu et al. \(2021\)](#), there still exists intractable challenges that prevent the model from becoming a universal vision backbone:

(1) These MLP-based approaches utilize fixed static matrices for patch communications or by manually-designed rules in a deterministic manner [Chen et al. \(2021\)](#), which is input

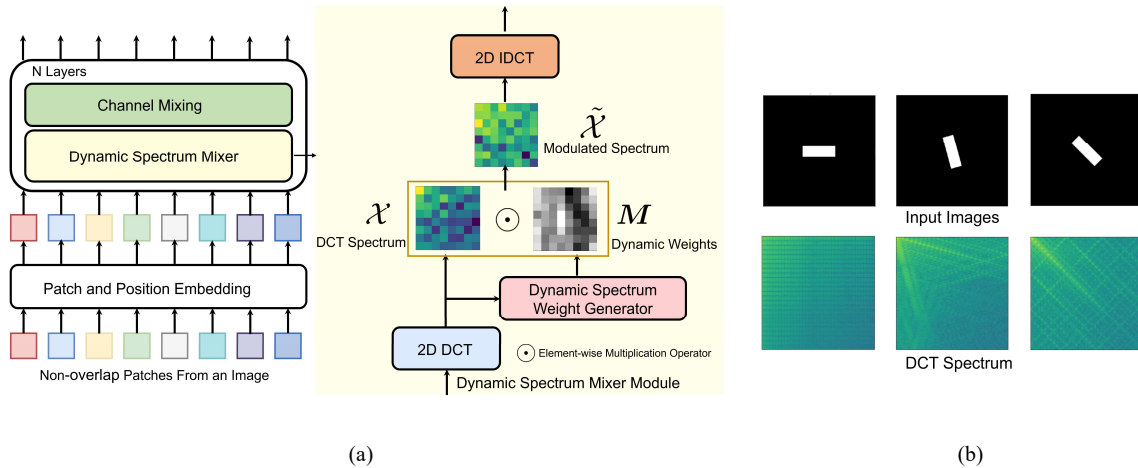


Figure 1: (a) The architecture of the proposed DSM. The proposed DSM mix the tokens in the frequency domain and empowers them with adaptability to the contents of tokens. (b) The input images and corresponding DCT spectrum. We can see that even rotating the image could cause a dramatic change in the frequency domain. The lighter the color, the larger the DCT spectrum weight

agnostic, restrict the adaptability to the contents to be fused, and lead to degradation of representability of learned feature.

(2) MLP-based ViT and its variations are excellent in capturing low-frequency visual data [Park and Kim \(2022\)](#), mostly global forms and structures of a scene or object, but they are less effective at learning high-frequency visual data, primarily local edges and textures. This is intuitively explained by the fact that the primary operation utilized in MLP to exchange information across non-overlap patch tokens, is a global operation and is far better equipped to capture global information (low frequencies) in the data than local information (high frequencies).

It has been demonstrated that the Fourier transforms might replace the multi-headed attention layers in transformers and produce equivalent performance. The FNet [Eckstein et al. \(2022\)](#), GFN [Rao et al. \(2021b\)](#), and AFNO [Guibas et al. \(2021\)](#), which mix the tokens by utilizing Fast Fourier Transform (FFT) in the frequency domain and achieve remarkable accuracy in visual recognition tasks. However, the GFN uses static global filters to exploit the long-term interaction information of spectrum tokens. The global filter is unchanged for different input images. We argue that, the image-agnostic global filter is not the optimal choice. We can see from the toy experiment in Fig. 1 (b), even rotating the image could cause a dramatic change in the frequency domain. Furthermore, these Fourier Transform-based methods treat all the spectrum equally, which is inefficient at capturing high frequencies that primarily carry local information, which prevents it from being used to the downstream dense prediction tasks.

In this paper, we attempt to address these issues mentioned above by seeking a way to project the spatial domain information into image-resolution agnostic transformed space, e.g., frequency domain. Specifically, we propose a dynamic frequency aggregation architecture with DCT and dynamically aggregating them concerning their contents. Each output from DCT has a component of each of the input tokens. Thus the proposed method can facilitate the information interaction across all tokens. In comparison to the DFT, the DCT is a real-valued transform that also breaks down a given signal or picture into its component frequency components. Therefore, in terms of computational cost, DCT is more suited for deep neural networks.

Furthermore, to adaptively amplify the useful frequency bands while downplaying others, we design a dynamic spectrum band attention module. Specifically, we propose simply down-sample the frequency feature to a pre-defined size for the images with variable resolutions and then calculating the attention weights of each spectrum band by using two layers of MLPs. We empirically find that frequency domain feature dimensions can be reduced significantly without sacrificing performance. The dimensions can even be shirked to a tiny number in our experiments. This finding enables us to employ MLPs to explore the rich relationships among spectrum tokens in a computationally efficient fashion. Overall, our contributions can be summarized as follows:

- We propose an MLP-like dynamic spectrum bands mixer, which could mix the tokens in the frequency domain and be empowered with adaptability to the contents of tokens.
- We developed an efficient spectrum band intersection module, which could capture the long-term dependency in a fixed-size down-sampled frequency domain without losing the universal approximating power. We also propose a Dynamic Spectrum Weight Generator (DSWG), which enhances the performance of ViT models by adaptively reweighting the high-frequency and low-frequency components with respect to the input image. The DSWG can learn representations of the global structure while filtering out frequency space data that is unrelated to the structure.
- We achieve 83.8% top-1 accuracy on ImageNet with 10.1G FLOPs, which significantly surpasses several MPL-like competitors. We also achieve consistent performance in other downstream tasks including object detection and semantic segmentation.

2. Related Works

2.1. Vision Transformer

Vision Transformer (ViT) [Dosovitskiy et al. \(2020\)](#) is the pioneering work that crops the entire image into 16×16 patches and treats each patch as a token as the input for the transformer. By utilizing an extremely largescale dataset, JFT-300M [Sun et al. \(2017\)](#), ViT has achieved promising performance comparable to CNN-based backbones. DeiT [Touvron et al. \(2021\)](#) further employs distillation and data augmentation techniques to improve the performance of ViT, without using an ultra-large-scale training dataset. The concurrent work, PVT [Wang et al. \(2021\)](#), and PiT [Heo et al. \(2021\)](#) exploit a feature pyramids architecture for vision transformers, which gradually down sampling the spatial dimension, making them more flexible for downstream dense prediction tasks. Han et al. propose TNT

Han et al. (2021) to model the attention information for the local patches for achieving better performance. To further enhance transferability, Swin Transformer, and Swin transformer v2 Liu et al. (2021b, 2022b) propose a new local attention paradigm that employs patch-level multi-head attention equipped with a hierarchical fusion design. Following this way, Shuffle Swin Transformer Huang et al. (2021) proposes shuffle multi-headed attention to reparametrize spatial connection between windows to improve the representation ability. Recently, DynamicViT Rao et al. (2021a) embraced the dynamic token sparing module with a vision-transformer and significantly increased the efficiency. Vision Transformer also shows its superiority on various downstream dense prediction tasks, e.g., object detection Carion et al. (2020), segmentation Cheng et al. (2022).

2.2. MLP-based Architectures

Global token-mixing MLPs: The pioneering work MLP-Mixer Tolstikhin et al. (2021) employs two Fully-Connected (FC) layers to fulfill the goal of communicating between tokens and achieving results that are comparable with ViT. gMLP Liu et al. (2021a) utilizes a gating operator to enhance the long-term interactions between different spatial locations. Recently, the Wave-MLP Tang et al. (2022) manually represents each token with two parts, amplitude, and phase, followed by a dynamic fusion operation. FNet Eckstein et al. (2022) first introduces Fourier Transform as the mixing mechanism and achieves excellent performance. A similar approach, Global Filter Network Rao et al. (2021b) also projects each token into the frequency domain by utilizing 2D FFT and then mixes the tokens in the frequency domain via a static global filter. However, the input-agnostic global filter hampers the representability of the model. In contrast, we propose to mix the spectrum tokens dynamically.

Local token-mixing MLPs: To enhance the efficiency of MLP-based token mixer, local token-mixing MLPs aim to invoke token mixing at the local region. AS-MLP Lian et al. (2021), S^2 -MLP and S^2 -MLPv2 Yu et al. (2022, 2021) perform spatial shift operations along the different axis to aggregate information from nearby tokens. CycleMLP Chen et al. (2021) and Morphmlp Zhang et al. (2021) propose mixing the local spatial information by employing hand-craft local kernels in a deterministic way. Hire-MLP Guo et al. (2022a) suggests hierarchically mixing the tokens to further enhance the representing ability. For the hybrid approach, ConvMLP Li et al. (2021) proposes a co-design of the convolution layer and MLP for the downstream dense prediction tasks.

2.3. Frequency Domain Learning

CNN-empowered Frequency domain learning has been successfully applied in multiple vision tasks, including Low-level vision such as JPEG image compression Gueguen et al. (2018), image super-resolution Magid et al. (2021), etc. Enhance the feature representations with global receptive fields Chi et al. (2020). Frequency domain attention is introduced by FcaNet Qin et al. (2021), which enhances the representability of ResNet He et al. (2016) on the image classification task. Specifically, the work proposed by Xu et al. in Xu et al. (2020) finds that the down-sampling in the frequency domain can better preserve image information than spatially resizing the images. This motivated us to derive frequency token interaction information in the down-sampled frequency domain.

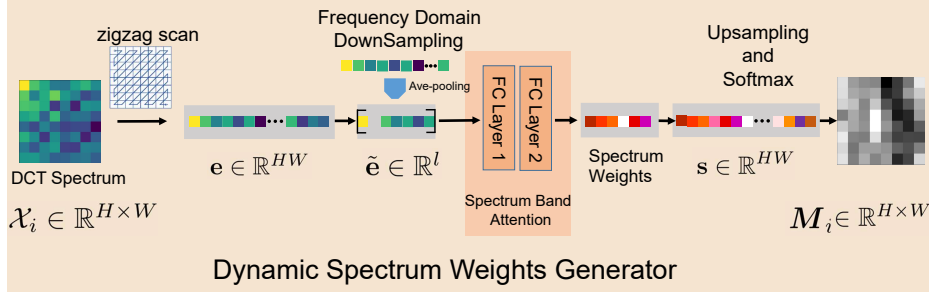


Figure 2: The diagram of the proposed Dynamic Spectrum Weights Generator

3. Approach

In this section, we present the proposed Dynamic Spectrum Mixer (DSM) in detail. After introducing the overall architecture briefly, we present the spectrum bands interaction module, which represents each token from the perspective of the DCT spectrum and reweights them in an input-adaptive manner. Finally, we introduce the architecture variants of the proposed DSM.

3.1. Preliminaries: Discrete Cosine Transform

DCT has been verified as a powerful tool in the image processing area, such as JPEG image compression, due to the properties of concentrating the energy of the image in several coefficients and decorrelating the coefficients. [Gueguen et al. \(2018\)](#). Mathematically, the two-dimensional (2D) DCT is formatted as follows:

$$B_{h,w}^{i,j} = \cos\left(\frac{\pi h}{H}\left(i + \frac{1}{2}\right)\right) \cos\left(\frac{\pi w}{W}\left(j + \frac{1}{2}\right)\right). \quad (1)$$

Then the 2D DCT for the input image with width W and height H is written by:

$$f_{h,w}^{2d} = \sum_{i=0}^{H-1} \sum_{j=0}^{W-1} I_{i,j}^{2d} B_{h,w}^{i,j} \quad (2)$$

s.t. $h \in \{0, 1, \dots, H-1\}, w \in \{0, 1, \dots, W-1\}$,

where $f^{2d} \in \mathbb{R}^{H \times W}$ is the 2D DCT frequency spectrum, $I^{2d} \in \mathbb{R}^{H \times W}$ is the input image, Accordingly, the inverse 2D DCT for the image is fomulated as:

$$I_{i,j}^{2d} = \sum_{h=0}^{H-1} \sum_{w=0}^{W-1} f_{h,w}^{2d} B_{h,w}^{i,j} \quad (3)$$

s.t. $i \in \{0, 1, \dots, H-1\}, j \in \{0, 1, \dots, W-1\}$.

The fast algorithm is [Makhoul \(1980\)](#) can be utilized to reduce the complexity of 1D-DCT from $\mathcal{O}(N^2)$ to $\mathcal{O}(N \log N)$. Due to the real-valued structure of the transform, the DCT and Inverse-DCT (IDCT) both have quick $\mathcal{O}(N \log N)$ algorithms that are quicker than FFT. Convolutions may be applied in the DCT domain using a modified form of the Fourier Convolution Theorem [Shen et al. \(1998\)](#).

3.2. Overall architecture

The overall architecture is constructed by stacking multiple DSM blocks, as shown in Fig. 1 (a). The basic element of DSM consists of 1) a forward DCT layer, which projects each token into the frequency domain; 2) a Dynamic Spectrum Weights Generator, which adaptively generates the global aggregating weights to modulated frequency features across spectrum bands and channels 3) an inverse DCT layer, which projects the frequency domain feature back to the spatial domain. The key module of the proposed architecture will be introduced in the following sector.

We first divide the input image into $H \times W$ non-overlapping patches and project the flattened patches into HW tokens with dimension D . Then perform whole image 2D DCT along the spatial dimensions to convert \mathbf{x} to the frequency domain:

$$\mathcal{X} = \mathcal{DCT}[\mathbf{X}] \in \mathbb{R}^{H \times W \times D}, \quad (4)$$

where $\mathcal{DCT}[\cdot]$ denotes the 2D DCT, \mathcal{X} is the spectrum of \mathbf{X} . We can then modulate the spectrum by multiplying a dynamic spectrum aggregator \mathbf{M} to the \mathcal{X} :

$$\tilde{\mathcal{X}} = \mathcal{X} \odot \mathbf{M}, \quad (5)$$

where \odot is the element-wise multiplication operator.

Finally, we project all the modulated frequency tensors back to the spatial domain by reverse DCT:

$$\hat{\mathbf{X}} = \mathcal{IDCT}[\tilde{\mathcal{X}}]. \quad (6)$$

3.3. Dynamic Spectrum Weights Generator (DSWG)

According to the property of DCT, a single output element from DCT has a component of each of the input tokens in the spatial domain. To this end, the goal of our DSWG module is to generate dynamic spectrum weights \mathbf{M} to modulate the transformed DCT frequency bands, which could facilitate the information intersection process reverses back to the spatial domain tokens. The process of dynamic spectrum weights generation is shown in Fig.2. Regarding the frequency bands tensor $\mathcal{X} \in \mathbb{R}^{W \times H \times C}$, we first equally split \mathcal{X} into C parts $\{\mathcal{X}_i\}_{i=1}^C$ along the channel dimension. Because the spectrum bands of DCT have clear physical meaning and which arranged from left to right and top to bottom in a strictly increasing order of frequencies. To this end, we can flat all the spectrum in $\mathcal{X}_i \in \mathbb{R}^{H \times W}$ into $\mathbf{e} \in \mathbb{R}^{HW}$ by using zigzag scan, and obtain the one-dimensional embedding.

Intuitively, we can employ multiple fully-connected layers to capture the full spectrum band interaction information. However, the computation complexity will be raised significantly to $\mathcal{O}(H^2W^2)$. To solve this problem, We argue that not all information in the frequency range has the perceptual ability. Many DCT-based methods introduce sparsity to DCT blocks through quantization Nash et al. (2021) or just drop the high-frequency part to reason the global dependency with redundancy elimination Liu et al. (2022a). Following this, as shown in Fig.3, we propose to only utilize the average-pooling operation over the inflated spectrum embedding \mathbf{e} . We downsampling the frequency band $\mathbf{e} \in \mathbb{R}^{HW}$ to $\tilde{\mathbf{e}} \in \mathbb{R}^l$. Then, a two-layer FC design is used to obtain the spectrum band attention weight, which can be formulated as follows:

$$\tilde{\mathbf{e}} \in \mathbb{R}^l = \mathbf{DownSampling}(\mathbf{zigzag}(\mathcal{X}_i)), \quad (7)$$

where *Trunc* and **zigzag** are truncation and zigzag scan operation, respectively.

$$\mathbf{s} \in \mathbb{R}^{HW} = \text{reshape}(\mathbf{W}_2 \sigma[\mathbf{W}_1 \text{LayerNorm}(\tilde{\mathbf{e}})]) \quad (8)$$

$$\hat{\mathbf{s}} = \text{softmax}(\mathbf{s}) \quad (9)$$

$$\mathbf{M}_i = \text{inverse} - \text{zigzag}(\text{UpSampling}(\hat{\mathbf{s}})) \quad (10)$$

where σ is the activation function implemented by Gaussian Error Linear Units (GELU) [Hendrycks and Gimpel \(2016\)](#), LayerNorm (\cdot) represents the layer normalization [Ba et al. \(2016\)](#), which is widely used in MLP-like token mixers. $\mathbf{W}_1 \in \mathbb{R}^{K \times l}$ denote the weights of a fully-connected layer, increasing the feature dimension from l to K where K is a fixed value. $\mathbf{W}_2 \in \mathbb{R}^{l \times K}$ refers to the weights of a fully-connected layer reshaping the feature from K back to the original dimension l .

Finally, the \mathbf{e} is further processed by *softmax* function and followed by inverse zigzag scanning mapping $\mathbb{R}^{HW} \mapsto \mathbb{R}^{H \times W}$ that reshape the embedding $\tilde{\mathbf{e}}$ back to get the dynamic spectrum weights \mathbf{M}_i . To generate a compact model, the mixing weight \mathbf{W}_1 and \mathbf{W}_2 are all shared for different channels.

3.4. Complexity Analysis

Thanks to the fast algorithm, the complexity of the DCT layer is $\mathcal{O}(HWC [\log_2(HW)])$, element-wise multiplication takes $\mathcal{O}(HWC)$, compared with standard self-attention $\mathcal{O}(HWC^2 + H^2W^2C)$. While the computation cost of DSWG is mainly from the two-layer FCs, with the truncated input $\mathcal{X} \in \mathbb{R}^{l \times C}$ and $\mathbf{W}_1 \in \mathbb{R}^{K \times l}$, $\mathbf{W}_2 \in \mathbb{R}^{l \times K}$, thus the computation complexity is $\mathcal{O}(Kl^2C + K^2lC)$.

3.5. Architecture Variants

Following the hierarchical architecture designs of previous works, e.g., Hire-MLP, [Guo et al. \(2022a\)](#), we introduce three four-stage variants of DSM architectures by varying the width and depth of the model and number of DSM blocks, denoted as ‘‘DSM-S’’, ‘‘DSM-M’’ and ‘‘DSM-L’’, respectively. ‘‘DSM-S’’ version has fewer layers for efficient implementation, while the ‘‘DSM-L’’ variant has a larger model size to achieve higher performance. The detailed architecture is provided in the supplemental material.

4. Experiments

To demonstrate the effectiveness of the proposed DSM architecture, we conduct experiments on a variety of tasks, including image classification, semantic segmentation ADE20K [Zhou et al. \(2019\)](#), and object detection COCO dataset [Lin et al. \(2014\)](#). Ablation investigations are then carried out to confirm the efficiency of each component. The experimental results are detailed in the following sections.

4.1. ImageNet-1K Classification

We evaluate the proposed DSM on the image classification task. The dataset ImageNet [Deng et al. \(2009\)](#) is utilized for benchmarking, which contains 1.28M training images and

Table 1: Comparison of the proposed DSM architecture with existing vision MLP models on ImageNet, the bold numbers are the results of the proposed method

Model	Params.	FLOPs	Throughput (image / s)	Top-1 acc. (%)
EAMLP-14 Guo et al. (2022b)	30M	-	771	78.9
Mixer-B/16 Tolstikhin et al. (2021)	59M	12.7G	-	76.4
ResMLP-S12 Touvron et al. (2022)	15M	3.0G	1415	76.6
ResMLP-S24 Touvron et al. (2022)	30M	6.0G	715	79.4
gMLP-S Liu et al. (2021a)	20M	4.5G	-	79.6
gMLP-B Liu et al. (2021a)	73M	15.8G	-	81.6
S ² -MLP-wide Yu et al. (2021)	71M	14.0G	-	80.0
S ² -MLP-deep Yu et al. (2021)	51M	10.5G	-	80.7
ViP-Small/7 Hou et al. (2022)	25M	6.9G	719	81.5
ViP-Large/7 Hou et al. (2022)	88M	24.4G	298	83.2
AS-MLP-T Lian et al. (2021)	28M	4.4G	862	81.3
AS-MLP-B Lian et al. (2021)	88M	15.2G	308	83.3
CycleMLP-B1 Chen et al. (2021)	15M	2.1G	1040	78.9
CycleMLP-B5 Chen et al. (2021)	76M	12.3G	253	83.2
S ² -MLPv2 Yu et al. (2022)	25M	6.9G	-	82.0
S ² -MLPv2 Yu et al. (2022)	55M	16.3G	-	83.6
Hire-MLP-Ti Guo et al. (2022a)	18M	2.1G	-	79.7
Hire-MLP-L Guo et al. (2022a)	96M	13.4G	-	83.8
ConvMLP-S Li et al. (2021)	9M	2.4G	-	76.8
ConvMLP-L Li et al. (2021)	43M	9.9G	-	80.2
Wave-MLP-T Tang et al. (2022)	15M	2.1G	1257	80.1
Wave-MLP-B Tang et al. (2022)	63M	10.2G	341	83.6
DSM-S (ours)	16M	2.4G	1218	80.2
DSM-M (ours)	30M	4.8G	701	82.7
DSM-L (ours)	90M	10.1G	338	83.8

over 50k validation images spread over 1000 classes. To make a fair comparison, we follow the training strategy in DeiT Touvron et al. (2021). Specifically, we train our model in 4 NVIDIA A100 GPUs by batch size 1024, and the DSM architecture is implemented by PyTorch. All the “DSM-S”, “DSM-M” and “DSM-L” models are trained for 300 epochs employing AdamW Loshchilov and Hutter (2017) optimizer, we set the initial learning rate as 2×10^{-3} and declines to 1×10^{-6} with a cosine decay strategy, and the weight decay is set to 0.05. The warming-up trick for the first 10 epochs is also utilized in our experiments. Moreover, We employ the data augmentation strategies following Touvron et al. (2021); Hou et al. (2022). The length of shrunk spectrum bands is set to be 16 for all the experiments.

Comparison with the existing MLP-like architectures. We compare our DSM with multiple MLP-like architectures, e.g., MLP-mixer Tolstikhin et al. (2021), gMLP Liu et al. (2021a), CycleMLP Chen et al. (2021), AS-MLP Lian et al. (2021), S²-MLP and S²-MLPv2 Yu et al. (2022, 2021), Hire-MLP Guo et al. (2022a). The results are listed in Table 1. We can see that, to reduce the computation complexity, the single scale-based approaches MLP-Mixer, ResMLP, gMLP, S2-MLP achieve inferior performance than the hierarchically-designed architecture, such as Hire-MLP and CycleMLP. In contrast, our method achieves a better trade-off between the computational cost and performance over the competitors. For

Table 2: Comparison of the proposed DSM architecture with SOTA models on ImageNet. The bold numbers are the results of the proposed method

Model	Family	Params.	FLOPs	Throughput (image / s)	Top-1 acc. (%)
ResNet18 He et al. (2016)	CNN	12M	1.8G	-	69.8
ResNet50 He et al. (2016)	CNN	26M	4.1G	-	78.5
RegNetY-4G Radosavovic et al. (2020)	CNN	21M	4.0G	1157	80.0
RegNetY-8G Radosavovic et al. (2020)	CNN	39M	8.0G	592	81.7
GFNet-H-S Rao et al. (2021b)	FFT	32M	4.5G	-	81.5
GFNet-H-B Rao et al. (2021b)	FFT	54M	8.4G	-	82.9
DeiT-S Touvron et al. (2021)	Trans	22M	4.6G	940	79.8
PVT-Small Wang et al. (2021)	Trans	25M	3.8G	820	79.8
PVT-Large Wang et al. (2021)	Trans	61M	9.8G	367	81.7
T2T-ViT-14 Yuan et al. (2021)	Trans	22M	5.2G	764	81.5
TNT-S Han et al. (2021)	Trans	24M	5.2G	428	81.5
TNT-B Han et al. (2021)	Trans	66M	14.1G	246	82.9
Swin-T Liu et al. (2021b)	Trans	29M	4.5G	755	81.3
Swin-S Liu et al. (2021b)	Trans	50M	8.7G	437	83.0
Swin-B Liu et al. (2021b)	Trans	88M	15.4G	278	83.5
DSM-S (ours)	DCT	16M	2.4G	1218	80.2
DSM-M (ours)	DCT	30M	4.8G	701	82.7
DSM-L (ours)	DCT	90M	10.1G	338	83.8

instance, with the large-size model DSM-L, compared with previous SOTA Hire-MLP-L [Guo et al. \(2022a\)](#) (83.8% accuracy, 13.4GFLOPs), our model also achieves the same accuracy (83.8%) with significantly similar parameters (90M vs. 96M) and FLOPs (10.1G vs. 13.4G). For the small-size models, our extremely tiny architecture DSM-S achieves 80.2% with only 16M parameters and 2.4G FLOPs, which constantly defeat the Hire-MLP-Ti [Guo et al. \(2022a\)](#), Wave-MLP-T [Tang et al. \(2022\)](#), and CycleMLP-B1 [Chen et al. \(2021\)](#). To this end, the effectiveness of the proposed spectrum mixing architecture is consolidated.

Comparisons with CNNs and vision Transformers. To further verify the performance of DSM, We compare the proposed DSM with major CNN and transformer-based architectures, the experimental results are shown in Table 2. We can see that our proposed DSM still constantly achieves the best accuracy compared to models with similar FLOPs. Specifically, compared with Swin Transformer [Liu et al. \(2021b\)](#), which is the state-of-the-art transformer architecture, our DSM obtains higher performance with fewer parameters and less computational complexity. For instance, our DMS-M, with 4.8G FLOPs, achieves 82.7% top-1 accuracy, which significantly surpasses the Swin-T (4.5G FLOPs) with 81.3% accuracy. This result consolidates that DSM architecture could empower the spectrum token aggregating process efficiently and achieve better performance. According to the above comparison results, we can see that DSM is a powerful architecture for visual recognition tasks.

Compared with FFT-based architecture GFNet The frequency domain token mixing architecture (GFNet-H-B) [Rao et al. \(2021b\)](#), which using static weights to argument all the spectrum, regardless of the input, we achieve 0.9% higher accuracy in Top-1 (82.9% vs. 83.8%). It is verified that equipping with the dynamic spectrum mixing strategy can

well capture the relationship between spectrum bands derived from input tokens than the static global filter.

4.2. Semantic Segmentation on ADE20K

Settings. To further verify the performance of our DSM, we conduct the semantic segmentation experiment on ADE20K [Zhou et al. \(2019\)](#), which contains 25k images from 150 semantic categories; among them, 20k are used for training, 2k for validation, and 3k for testing. To compare the results fairly, we also adhere to the training guidelines used by the earlier versions of the vision Transformers [Chen et al. \(2021\)](#) for the Semantic FPN [Kirillov et al. \(2019\)](#) and UperNet [Xiao et al. \(2018\)](#) frameworks. The models have been trained using ImageNet-1k with input image size 224×224 and then retrained on ADE20K with a resolution of 512×512 . For training the Semantic FPN, we utilize the AdamW optimizer with a learning rate 1.25×10^{-4} and weight decay set to be 0.0001. The Semantic FPN is trained for 40K iterations with a batch size of 32.

For the UperNet framework, we train the models for 160K iterations. AdamW optimizer is employed with the learning rate 4.25×10^{-5} , weight decay 0.01, and batch size is set to 16. The mIoU is then tested using single-scale and multi-scale (MS), where the scale ranges from 0.5 to 1.75 with a 0.25-interval.

Results. The output from several models for semantic segmentation is displayed in Table 3. Our DSM consistently performs better than the latest models under various parameters and computational configurations. DSM demonstrates a considerable advantage when compared to transformer-based models like PVT, for example, achieving 4.6 percent higher mIoU. Furthermore, it surpasses the Swin-S model and the CycleMLP-B2 by a large margin.

Additionally, we employ another widely used framework, UperNet [Xiao et al. \(2018\)](#), as a backbone for our DSM validation by following [Liu et al. \(2021b\)](#). In comparison to the most advanced Swin Transformer [Liu et al. \(2021b\)](#), the result suggested DSM outperforms the state-of-the-art Swin Transformer [Liu et al. \(2021b\)](#) in terms of MS mIoU and outperforms Swin-T by +1.7 mIoU in terms of SS mIoU. We conclude that aggregating various tokens in the frequency domain can capture more comprehensive information and hence improve the semantic segmentation performance.

4.3. Object Detection on COCO

Settings. We perform the object detection and instance segmentation tests using the COCO 2017 benchmark [Lin et al. \(2014\)](#), which includes 118K training pictures and 5K validation images. Two popular detectors, RetinaNet [Lin et al. \(2017\)](#) and Mask R-CNN [He et al. \(2017\)](#), both employ DSM as their backbone. We train the model using the AdamW [Loshchilov and Hutter \(2017\)](#) optimizer for 12 epochs following the training recipe in [Wang et al. \(2021\)](#) to ensure a fair comparison. The resized images are used to train models, with the longest side being no more than 1333 pixels and the shorter side ranging from 480 to 800 pixels. the batch size is set as 16 with a starting learning rate of 0.0001. While the backbones are initialized with pre-trained weights from ImageNet.

Results. In Table 4, we provide the object identification and instance segmentation results obtained using various training schedules and frameworks. According to Table 4, under comparable FLOPs limitations, when compared to the current models, DSM-based RetinaNet

Table 3: ADE20K validation set semantic segmentation results. A 2048×512 input size is used to calculate FLOPs, and the results come from GFNet, as indicated by the \dagger symbol.

Semantic FPN						UperNet				
Backbone	Param	FLOPs	FPS	ISS mIoU	Backbone	Param	FLOPs	FPS	ISS mIoU	MS mIoU
PVT-Small	28M	163G	43.9	39.8	Swin-T	60M	945G	18.5	44.5	46.1
CycleMLP-B2	31M	167G	44.5	42.4	AS-MLP-T	60M	937G	17.7	-	46.5
Hire-MLP-Small	37M	174G	47.3	44.3	Hire-MLP-Small	63M	930G	19.3	46.1	47.1
DSM-S(ours)	36M	169G	48.2	44.4	DSM-S(ours)	60M	908G	21.2	46.2	47.3
CycleMLP-B3	42M	229G	31.0	44.5	ResNet-101	86M	1029G	20.1	43.8	44.9
GFNet-Base	75M	261G	-	44.8	Swin-S	81M	1038G	15.2	47.6	49.5
CycleMLP-B4	56M	296G	23.6	45.1	AS-MLP-S	81M	1024G	14.4	-	49.2
Hire-MLP-Base	62M	255G	31.8	46.2	Hire-MLP-Base	88M	1011G	16.0	48.3	49.6
DSM-M(ours)	66M	258G	30.3	46.4	DSM-M(ours)	90M	1100G	15.1	48.4	49.7
Swin-B	53M	274G	23.4	45.2 \dagger	Swin-B	121M	1188G	13.3	48.1	49.7
CycleMLP-B5	79M	343G	22.9	45.6	AS-MLP-B	121M	1166G	11.0	-	49.5
Hire-MLP-Large	99M	366G	24.5	46.6	Hire-MLP-Large	127M	1125G	13.7	48.8	49.9
DSM-L(ours)	93M	349G	24.9	46.8	DSM-L(ours)	119M	1109G	13.9	48.9	49.9

Table 4: Results of object detection and instance segmentation on COCO val2017.

Backbone	RetinaNet 1x							Mask R-CNN 1x						
	Params. / FLOPs	AP	AP ₅₀	AP ₇₅	AP _S	AP _M	AP _L	Params. / FLOPs	AP ^b	AP ₅₀ ^b	AP ₇₅ ^b	AP ^m	AP ₅₀ ^m	AP ₇₅ ^m
ResNet50	37.7M / 239.3G	36.3	55.3	38.6	19.3	40.0	48.8	44.2M / 260.1G	38.0	58.6	41.4	34.4	55.1	36.7
Swin-T	38.5M / 244.8G	41.5	62.1	44.2	25.1	44.9	55.5	47.8M / 264.0G	42.2	64.6	46.2	39.1	61.6	42.0
PVT-Small	34.2M / 226.5G	40.4	61.3	43.0	25.0	42.9	55.7	44.1M / 245.1G	40.4	62.9	43.8	37.8	60.1	40.3
CycleMLP-B2	36.5M / 230.9G	40.9	61.8	43.4	23.4	44.7	53.4	46.5M / 249.5G	41.7	63.6	45.8	38.2	60.4	41.0
Wave-MLP-S	37.1M / 231.3G	43.4	64.4	46.5	26.6	47.1	57.1	47.0M / 250.3G	44.0	65.8	48.2	40.0	63.1	42.9
DSM-S(ours)	35.1M / 219.2G	43.5	65.5	46.6	26.6	47.2	57.3	46.2M / 248.1G	44.1	65.6	48.4	40.1	63.2	42.9
ResNet101	56.7M / 315.4G	38.5	57.8	41.2	21.4	42.6	51.1	63.2M / 336.4G	40.4	61.1	44.2	36.4	57.7	38.8
Swin-S	59.8M / 334.8G	44.5	65.7	47.5	27.4	48.0	59.9	69.1M / 353.8G	44.8	66.6	48.9	40.9	63.4	44.2
PVT-Medium	53.9M / 283.1G	41.9	63.1	44.3	25.0	44.9	57.6	63.9M / 301.7G	42.0	64.4	45.6	39.0	61.6	42.1
CycleMLP-B3	48.1M / 291.3G	42.5	63.2	45.3	25.2	45.5	56.2	58.0M / 309.9G	43.4	65.0	47.7	39.5	62.0	42.4
Wave-MLP-M	49.4M / 291.3G	44.8	65.8	47.8	28.0	48.2	59.1	59.6M / 311.5G	45.3	67.0	49.5	41.0	64.1	44.1
DSM-M(ours)	48.1M / 288.1G	44.9	65.9	47.9	26.6	48.3	59.4	58.6M / 252.1G	45.4	67.2	49.4	41.1	64.2	44.3
PVT-Large	71.1M / 345.7G	42.6	63.7	45.4	25.8	46.0	58.4	81.0M / 364.3G	42.9	65.0	46.6	39.5	61.9	42.5
CycleMLP-B4	61.5M / 356.6G	43.2	63.9	46.2	26.6	46.5	57.4	71.5M / 375.2G	44.1	65.7	48.1	40.2	62.7	43.5
CycleMLP-B5	85.9M / 402.2G	42.7	63.3	45.3	24.1	46.3	57.4	95.3M / 421.1G	44.1	65.5	48.4	40.1	62.8	43.0
Wave-MLP-B	66.1M / 333.9G	44.2	65.1	47.1	27.1	47.8	58.9	75.1M / 353.2G	45.7	67.5	50.1	27.8	49.2	59.7
DSM-L(ours)	64.1M / 300.1G	44.1	65.4	47.3	27.4	47.9	59.0	71.0M / 348.3G	45.7	67.7	50.3	41.7	64.7	45.4

and Mask R-CNN, consistently outperform CNN-based ResNet, transformer-based PVT, and MLP-based CycleMLP. Using RetinaNet as the backbone, our DSM-S consistently outperforms ResNet50 and CycleMLP-B2, bringing +7.2 AP gains over ResNets and +2.6 AP gains over CycleMLP-B2 with significantly greater model size and FLOPs. As demonstrated in Table 4, DSM-M-based Cascade Mask R-CNN outperforms Wave-MLP-M in both box AP and mask AP with fewer FLOPs. Our DSM achieves much greater performance (45.4 box AP and 41.1 mask AP) with fewer parameters (58.6M) and lower computational cost (252.1G) than Swin-S, which has 44.8 box AP and 40.9 mask AP with 69.1M parameters and 353.8G FLOPs. According to the findings, DSM may make a fantastic foundation for object identification.

5. Ablation Studies

Table 5: Ablation Study on Dynamic Spectrum Weight.

Model	generating methods	Top-1 (%)
DSM-S	Random Weight	70.5
DSM-S	All-pass Filter	76.4
DSM-S	DSM-Dynamic	80.2

Table 6: Ablation Study on Spectrum Length for DSM-S model.

Length	Params.	FLOPs	Top-1 accuracy (%)
4×4	12M	1.8G	72.7
8×8	15M	2.1G	76.9
10×10	16M	2.4G	80.2
12×12	16.4M	3.8G	80.3
16×16	16.8M	6.9G	80.3
All	18M	8.3G	80.4

5.1. The Effectiveness of Dynamic Spectrum Weight

To evaluate the effectiveness of the proposed Dynamic Spectrum Weight generator module, we designed three versions of experiments. (1) Only using the random values as the spectrum mixing weight. (2) All-pass filter, i.e., set all the weights to 1, left the spectrum untouched. In other words, merely utilize original 2D DCT to mix all the tokens, a similar way to FNet [Eckstein et al. \(2022\)](#). (3) Our Dynamic Spectrum Weight generator. The comparison results are listed in Table 5. We can see that the random weight leads to significant performance degradation (70.5% Top-1), while the all-pass filter achieves much better accuracy than the random one. Among all the weight generation mechanisms, our DSM demonstrates the best performance. This result verifies that the dynamically generated spectrum weight empowers the token mixer with improved representation ability.

5.2. Influence of the Spectrum Length

To evaluate the influence of spectrum length l on the performance, We compare the performance of several settings in Table 6 on ImageNet-1K. Intuitively, the longer spectrum length is beneficial to fine-grained modeling details of the input tokens and tends to achieve higher recognition accuracy. Surprisingly, as shown in the table, even employing only 8×8 spectrum bands can achieve 76.9% accuracy. As the length grows from 32 to 64, the accuracy remains unchanged. This result confirms that compressed DCT spectrums can reduce the computation cost for the proposed DSM without sacrificing accuracy.

6. Conclusion

We propose a dynamic token mixing architecture in the frequency domain for the visual recognition task, representing each token as a DCT spectrum. With the dynamically generated weight, all the tokens are aggregated with varying contents from different input images. Extensive experiments show that the proposed DSM outperforms the existing MLP-like architectures and can also be used as a strong backbone for the image classification task. In the future, we will further explore the DSM architecture for downstream dense prediction tasks, such as object detection and semantic segmentation.

References

- Jimmy Lei Ba, Jamie Ryan Kiros, and Geoffrey E Hinton. Layer normalization. *arXiv preprint arXiv:1607.06450*, 2016.
- Nicolas Carion, Francisco Massa, Gabriel Synnaeve, Nicolas Usunier, Alexander Kirillov, and Sergey Zagoruyko. End-to-end object detection with transformers. In *European conference on computer vision*, pages 213–229. Springer, 2020.
- Shoufa Chen, Enze Xie, Chongjian Ge, Ding Liang, and Ping Luo. Cyclemlp: A mlp-like architecture for dense prediction. *arXiv preprint arXiv:2107.10224*, 2021.
- Bowen Cheng, Ishan Misra, Alexander G Schwing, Alexander Kirillov, and Rohit Girdhar. Masked-attention mask transformer for universal image segmentation. In *Proceedings of the IEEE/CVF Conference on Computer Vision and Pattern Recognition*, pages 1290–1299, 2022.
- Lu Chi, Borui Jiang, and Yadong Mu. Fast fourier convolution. *Advances in Neural Information Processing Systems*, 33:4479–4488, 2020.
- Jia Deng, Wei Dong, Richard Socher, Li-Jia Li, Kai Li, and Li Fei-Fei. Imagenet: A large-scale hierarchical image database. In *2009 IEEE conference on computer vision and pattern recognition*, pages 248–255. Ieee, 2009.
- Alexey Dosovitskiy, Lucas Beyer, Alexander Kolesnikov, Dirk Weissenborn, Xiaohua Zhai, Thomas Unterthiner, Mostafa Dehghani, Matthias Minderer, Georg Heigold, Sylvain Gelly, et al. An image is worth 16x16 words: Transformers for image recognition at scale. *arXiv preprint arXiv:2010.11929*, 2020.
- Ilya Eckstein, James Patrick Lee-Thorp, Joshua Ainslie, and Santiago Ontanon. Fnet: Mixing tokens with fourier transforms. 2022.
- Lionel Gueguen, Alex Sergeev, Ben Kadlec, Rosanne Liu, and Jason Yosinski. Faster neural networks straight from jpeg. *Advances in Neural Information Processing Systems*, 31, 2018.
- John Guibas, Morteza Mardani, Zongyi Li, Andrew Tao, Anima Anandkumar, and Bryan Catanzaro. Adaptive fourier neural operators: Efficient token mixers for transformers. *arXiv preprint arXiv:2111.13587*, 2021.
- Jianyuan Guo, Yehui Tang, Kai Han, Xinghao Chen, Han Wu, Chao Xu, Chang Xu, and Yunhe Wang. Hire-mlp: Vision mlp via hierarchical rearrangement. In *Proceedings of the IEEE/CVF Conference on Computer Vision and Pattern Recognition*, pages 826–836, 2022a.
- Meng-Hao Guo, Zheng-Ning Liu, Tai-Jiang Mu, and Shi-Min Hu. Beyond self-attention: External attention using two linear layers for visual tasks. *IEEE Transactions on Pattern Analysis and Machine Intelligence*, 2022b.
- Kai Han, An Xiao, Enhua Wu, Jianyuan Guo, Chunjing Xu, and Yunhe Wang. Transformer in transformer. *Advances in Neural Information Processing Systems*, 34:15908–15919, 2021.
- Kaiming He, Xiangyu Zhang, Shaoqing Ren, and Jian Sun. Deep residual learning for image recognition. In *Proceedings of the IEEE conference on computer vision and pattern recognition*, pages 770–778, 2016.
- Kaiming He, Georgia Gkioxari, Piotr Dollár, and Ross Girshick. Mask r-cnn. In *Proceedings of the IEEE international conference on computer vision*, pages 2961–2969, 2017.

- Dan Hendrycks and Kevin Gimpel. Gaussian error linear units (gelus). *arXiv preprint arXiv:1606.08415*, 2016.
- Byeongho Heo, Sangdoon Yun, Dongyoon Han, Sanghyuk Chun, Junsuk Choe, and Seong Joon Oh. Rethinking spatial dimensions of vision transformers. In *Proceedings of the IEEE/CVF International Conference on Computer Vision*, pages 11936–11945, 2021.
- Qibin Hou, Zihang Jiang, Li Yuan, Ming-Ming Cheng, Shuicheng Yan, and Jiashi Feng. Vision permutator: A permutable mlp-like architecture for visual recognition. *IEEE Transactions on Pattern Analysis and Machine Intelligence*, 2022.
- Zilong Huang, Youcheng Ben, Guozhong Luo, Pei Cheng, Gang Yu, and Bin Fu. Shuffle transformer: Rethinking spatial shuffle for vision transformer. *arXiv preprint arXiv:2106.03650*, 2021.
- Alexander Kirillov, Ross Girshick, Kaiming He, and Piotr Dollár. Panoptic feature pyramid networks. In *Proceedings of the IEEE/CVF Conference on Computer Vision and Pattern Recognition*, pages 6399–6408, 2019.
- Jiachen Li, Ali Hassani, Steven Walton, and Humphrey Shi. Convmlp: Hierarchical convolutional mlps for vision. *arXiv preprint arXiv:2109.04454*, 2021.
- Dongze Lian, Zehao Yu, Xing Sun, and Shenghua Gao. As-mlp: An axial shifted mlp architecture for vision. *arXiv preprint arXiv:2107.08391*, 2021.
- Tsung-Yi Lin, Michael Maire, Serge Belongie, James Hays, Pietro Perona, Deva Ramanan, Piotr Dollár, and C Lawrence Zitnick. Microsoft coco: Common objects in context. In *European conference on computer vision*, pages 740–755. Springer, 2014.
- Tsung-Yi Lin, Priya Goyal, Ross Girshick, Kaiming He, and Piotr Dollár. Focal loss for dense object detection. In *Proceedings of the IEEE international conference on computer vision*, pages 2980–2988, 2017.
- Hanxiao Liu, Zihang Dai, David So, and Quoc V Le. Pay attention to mlps. *Advances in Neural Information Processing Systems*, 34:9204–9215, 2021a.
- Hao Liu, Xinghua Jiang, Xin Li, Zhimin Bao, Deqiang Jiang, and Bo Ren. Nommer: Nominate synergistic context in vision transformer for visual recognition. In *Proceedings of the IEEE/CVF Conference on Computer Vision and Pattern Recognition*, pages 12073–12082, 2022a.
- Ze Liu, Yutong Lin, Yue Cao, Han Hu, Yixuan Wei, Zheng Zhang, Stephen Lin, and Baining Guo. Swin transformer: Hierarchical vision transformer using shifted windows. In *Proceedings of the IEEE/CVF International Conference on Computer Vision*, pages 10012–10022, 2021b.
- Ze Liu, Han Hu, Yutong Lin, Zhuliang Yao, Zhenda Xie, Yixuan Wei, Jia Ning, Yue Cao, Zheng Zhang, Li Dong, et al. Swin transformer v2: Scaling up capacity and resolution. In *Proceedings of the IEEE/CVF Conference on Computer Vision and Pattern Recognition*, pages 12009–12019, 2022b.
- Ilya Loshchilov and Frank Hutter. Decoupled weight decay regularization. *arXiv preprint arXiv:1711.05101*, 2017.
- Salma Abdel Magid, Yulun Zhang, Donglai Wei, Won-Dong Jang, Zudi Lin, Yun Fu, and Hanspeter Pfister. Dynamic high-pass filtering and multi-spectral attention for image super-resolution. In *Proceedings of the IEEE/CVF International Conference on Computer Vision*, pages 4288–4297, 2021.

- John Makhoul. A fast cosine transform in one and two dimensions. *IEEE Transactions on Acoustics, Speech, and Signal Processing*, 28(1):27–34, 1980.
- Charlie Nash, Jacob Menick, Sander Dieleman, and Peter W Battaglia. Generating images with sparse representations. *arXiv preprint arXiv:2103.03841*, 2021.
- Namuk Park and Songkuk Kim. How do vision transformers work? *arXiv preprint arXiv:2202.06709*, 2022.
- Zequn Qin, Pengyi Zhang, Fei Wu, and Xi Li. Fcanet: Frequency channel attention networks. In *Proceedings of the IEEE/CVF international conference on computer vision*, pages 783–792, 2021.
- Ilija Radosavovic, Raj Prateek Kosaraju, Ross Girshick, Kaiming He, and Piotr Dollár. Designing network design spaces. In *Proceedings of the IEEE/CVF conference on computer vision and pattern recognition*, pages 10428–10436, 2020.
- Yongming Rao, Wenliang Zhao, Benlin Liu, Jiwen Lu, Jie Zhou, and Cho-Jui Hsieh. Dynamicvit: Efficient vision transformers with dynamic token sparsification. *Advances in neural information processing systems*, 34:13937–13949, 2021a.
- Yongming Rao, Wenliang Zhao, Zheng Zhu, Jiwen Lu, and Jie Zhou. Global filter networks for image classification. *Advances in Neural Information Processing Systems*, 34:980–993, 2021b.
- Bo Shen, Ishwar K Sethi, and Vasudev Bhaskaran. Dct convolution and its application in compressed domain. *IEEE transactions on circuits and systems for video technology*, 8(8):947–952, 1998.
- Chen Sun, Abhinav Shrivastava, Saurabh Singh, and Abhinav Gupta. Revisiting unreasonable effectiveness of data in deep learning era. In *Proceedings of the IEEE international conference on computer vision*, pages 843–852, 2017.
- Yehui Tang, Kai Han, Jianyuan Guo, Chang Xu, Yanxi Li, Chao Xu, and Yunhe Wang. An image patch is a wave: Phase-aware vision mlp. In *Proceedings of the IEEE/CVF Conference on Computer Vision and Pattern Recognition*, pages 10935–10944, 2022.
- Ilya O Tolstikhin, Neil Houlsby, Alexander Kolesnikov, Lucas Beyer, Xiaohua Zhai, Thomas Unterthiner, Jessica Yung, Andreas Steiner, Daniel Keysers, Jakob Uszkoreit, et al. Mlp-mixer: An all-mlp architecture for vision. *Advances in Neural Information Processing Systems*, 34:24261–24272, 2021.
- Hugo Touvron, Matthieu Cord, Matthijs Douze, Francisco Massa, Alexandre Sablayrolles, and Hervé Jégou. Training data-efficient image transformers & distillation through attention. In *International Conference on Machine Learning*, pages 10347–10357. PMLR, 2021.
- Hugo Touvron, Piotr Bojanowski, Mathilde Caron, Matthieu Cord, Alaaeldin El-Nouby, Edouard Grave, Gautier Izacard, Armand Joulin, Gabriel Synnaeve, Jakob Verbeek, et al. Resmlp: Feedforward networks for image classification with data-efficient training. *IEEE Transactions on Pattern Analysis and Machine Intelligence*, 2022.
- Ashish Vaswani, Noam Shazeer, Niki Parmar, Jakob Uszkoreit, Llion Jones, Aidan N Gomez, Lukasz Kaiser, and Illia Polosukhin. Attention is all you need. *Advances in neural information processing systems*, 30, 2017.
- Wenhai Wang, Enze Xie, Xiang Li, Deng-Ping Fan, Kaitao Song, Ding Liang, Tong Lu, Ping Luo, and Ling Shao. Pyramid vision transformer: A versatile backbone for dense prediction without convolutions. In *Proceedings of the IEEE/CVF International Conference on Computer Vision*, pages 568–578, 2021.

- Tete Xiao, Yingcheng Liu, Bolei Zhou, Yuning Jiang, and Jian Sun. Unified perceptual parsing for scene understanding. In *Proceedings of the European Conference on Computer Vision (ECCV)*, 2018.
- Kai Xu, Minghai Qin, Fei Sun, Yuhao Wang, Yen-Kuang Chen, and Fengbo Ren. Learning in the frequency domain. In *Proceedings of the IEEE/CVF Conference on Computer Vision and Pattern Recognition*, pages 1740–1749, 2020.
- Tan Yu, Xu Li, Yunfeng Cai, Mingming Sun, and Ping Li. S²-mlpv2: Improved spatial-shift mlp architecture for vision. *arXiv preprint arXiv:2108.01072*, 2021.
- Tan Yu, Xu Li, Yunfeng Cai, Mingming Sun, and Ping Li. S2-mlp: Spatial-shift mlp architecture for vision. In *Proceedings of the IEEE/CVF Winter Conference on Applications of Computer Vision*, pages 297–306, 2022.
- Li Yuan, Yunpeng Chen, Tao Wang, Weihao Yu, Yujun Shi, Zi-Hang Jiang, Francis EH Tay, Jiashi Feng, and Shuicheng Yan. Tokens-to-token vit: Training vision transformers from scratch on imagenet. In *Proceedings of the IEEE/CVF International Conference on Computer Vision*, pages 558–567, 2021.
- David Junhao Zhang, Kunchang Li, Yunpeng Chen, Yali Wang, Shashwat Chandra, Yu Qiao, Luoqi Liu, and Mike Zheng Shou. Morphmlp: A self-attention free, mlp-like backbone for image and video. *arXiv preprint arXiv:2111.12527*, 2021.
- Bolei Zhou, Hang Zhao, Xavier Puig, Tete Xiao, Sanja Fidler, Adela Barriuso, and Antonio Torralba. Semantic understanding of scenes through the ade20k dataset. *International Journal of Computer Vision*, 2019.